Design considerations and electro-mechanical simulation of an inertial sensor based on a floating gate metal-oxide semiconductor field-effect transistor as transducer

G. S. Abarca Jiménez, M. A. Reyes Barranca, S. Mendoza Acevedo, J. E. Munguía Cervantes & M. A. Alemán Arce

Springer

Springer

TECHNICAL PAPER

Design considerations and electro-mechanical simulation of an inertial sensor based on a floating gate metal-oxide semiconductor field-effect transistor as transducer

**G. S. Abarca Jiménez · M. A. Reyes Barranca ·
S. Mendoza Acevedo · J. E. Munguía Cervantes ·
M. A. Alemán Arce**

Abstract   In this paper, an analysis on the electrostatic actuation in capacitive complementary metal-oxide semiconductor and micro-electro-mechanical systems (CMOS–MEMS) inertial sensors is presented. These sensors are designed to be used in combination with a floating gate metal oxide semiconductor field-effect transistor as the transducer to convert inertial force to an electrical signal. The effects of connecting micro-sensors with different geometry and having the same mechanic characteristics and integrated electronics for transducing are analyzed. It is shown that the performance of these capacitive structures depends mainly on features like the mechanical properties of the material used and the mechanical behavior given by the geometry. Undesired effects like pitch, roll and yaw movements depend on the geometry and the configuration of the proposed capacitive structure. Also, the biasing of the transducer included in the system affects the electrostatic actuation of the inertial sensor. This study shows that some geometric designs of this kind of sensors may result unreliable for a good transduction when an external force is applied. Furthermore, the proposed design can be fabricated using standard CMOS technologies followed by a sacrificial layer surface micromachining needed for the structure release.

G. S. Abarca Jiménez (✉) · M. A. Reyes Barranca
Department of Electrical Engineering, CINVESTAV-IPN,
Av. Instituto Politécnico Nacional 2508, 07360 Mexico, Mexico
e-mail: gabarca@cinvestav.mx

S. Mendoza Acevedo
Centro de Investigación en Computación- Instituto Politécnico
Nacional, Av. Juan de Dios Bátiz, and Av. Miguel Othón de
Mendizábal, 07738 Mexico, Mexico

J. E. Munguía Cervantes · M. A. Alemán Arce
Centro de Nanociencias y Micro y Nano Tecnologías- Instituto
Politécnico Nacional, Luis Enrique Erro s/n,
07738 Mexico, Mexico

1 Introduction

Since there are several similar fabrication steps in micro-electro-mechanical systems (MEMS) and complementary metal-oxide semiconductor (CMOS) technologies, a derivative technology has been called CMOS–MEMS (Lazarus et al. 2010); from this technology the sensors and actuators are fabricated together with the electronics in the same substrate, hence, micromachining post–processes are made once the chip is completed by the foundry. This approach presents several advantages, however, a disadvantage arises when CMOS–MEMS technology is used; the layers used for the integrated circuits fabrication are thinner than those used in MEMS dedicated technologies like Multi-User MEMS Processes (MUMPs) (Khan et al. 2013), Silicon-On-Insulator MEMS (SOI-MEMS) (Andò et al. 2011), Lithography, Electroplating, Molding (LIGA) (Hsu et al. 2012), and others. The main characteristic of CMOS–MEMS fabrication is compatibility with microelectronics processes. No matter what kind of technology is used, MEMS sensors provide lower power consumption, as well as compact and robust design.

Miniaturization in MEMS sensors not only allows for small areas, but also applies for better resonance frequencies (Sethuramalingam and Vilmalajuliet 2010). For this reason, it is critical to have good understanding of the scaling properties of the transduction mechanism, the overall design, the materials used in the fabrication of the structure and the fabrication processes involved.

The sensitivity in inertial MEMS capacitive sensors is inversely proportional to the spring constant (Mukherjee et al. 2011) of the beams that support the proof mass to the frame of the device. In this work, in order to improve the sensitivity in CMOS–MEMS inertial sensors, different

geometries are shown, using Floating Gate MOS transistors as transducers; the results of the mechanical and electro–mechanical analysis of different capacitive structures are presented.

As this study uses a FGMOS as a transducer element, the capacitive structure may present unwanted electrostatic actuation due to the voltage needed to establish the operating region of the transistor regarding the coupling capacitance of the FGMOS forms part of the inertial sensor. As mentioned, when using standard CMOS technology, the layers available for making structures are very thin compared with dedicated technologies for MEMS, which is reflected in undesirable effect like roll, pitch and yaw movements, not only because of the mentioned unwanted electrostatic actuation, but also by the inertial force applied for which the sensor is designed. The derived consequence is that these added movements change the equivalent capacitance of the circuit inducing noise in the measurement.

This work focuses on the performance simulation and analysis of an accelerometer designed with particular capacitive structures, evaluating parameters like displacement due to an applied force, stress capability of the springs used and the derived pull–in voltage before the capacitor plates stick together, so the structure can be electrostatically tested for reliable movement. The analysis presented in this work was made using COMSOL® for simulation of the structure under different conditions and the results are shown in the following sections.

2 The inertial sensor and the FGMOS

The capacitive structure for the devices described in this work is calculated based on design rules of a standard CMOS process (On Semiconductor 0.5 microns, N–well, double polysilicon, three metal layers). Thereby, thanks to the double layer of polysilicon offered by this technology, FGMOS transistors can be fabricated. Normally, this device uses the top polysilicon layer as a control gate and the bottom polysilicon layer underneath it operates as the floating gate. When a voltage is applied to the control gate an electric field is present over the floating gate owing to the capacitive coupling existing between the control gate and the floating gate. Hence, the current flowing along the channel will depend on the apparent voltage present over the floating gate, which in turn is a function of the coupling coefficient given by the total capacitance of the device. This structure will provide a convenient change in capacitance resulting in a reliable coupling coefficient for the FGMOS to operate as a transducer. This can be achieved since the capacitor plates which determine the coupling coefficient, typical of the
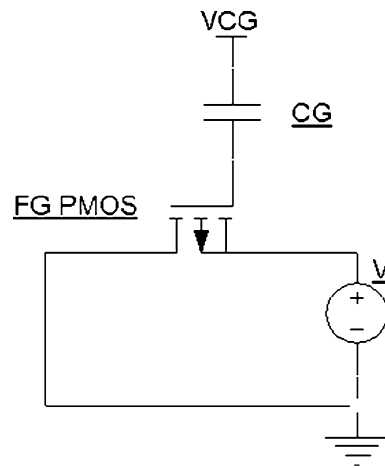

Fig. 1 Equivalent circuit of the variable coupling coefficient

FGMOS, are part of the inertial sensor, as well, where one plate is fixed and the other has a displacement when a force is applied to the system. The equivalent circuit is shown in Fig. 1. The variable capacitor C_G is formed by the seismic and fixed masses as the plates of the capacitor and air as dielectric.

When the device is subjected to acceleration, the distance between the capacitor plates either increases or decreases, changing the capacitive value. This change has an effect over the behavior of the FGMOS, changing the voltage over the floating gate (V_{FG}); if the transistor is operating in the saturation region, this change can be calculated by (1):

$$V_{FG} = K_{CG}V_{CG} + \frac{C_D}{C_{TOT}}V_D + \frac{C_S}{C_{TOT}}V_S$$
$$+ \frac{C_{FOX}}{C_{TOT}}V_B + \frac{C_{OX}}{C_{TOT}}V_G + \frac{Q_{FG}}{C_{TOT}} \quad (1)$$

where

$$K_{CG} = \frac{C_G}{C_{TOT}} \quad (2)$$

$$C_{TOT} = C_G + C_D + C_S + C_{FOX} + C_{OX} \quad (3)$$

where C_G is the capacitor due to the capacitive structure, V_{CG} is the control gate voltage, V_{FG} is the voltage on the floating gate, C_{TOT} is the total equivalent capacitance, V_D is the drain voltage, C_D is the parasitic capacitance formed by the drain and the floating gate, C_S is the parasitic capacitance between the source and the floating gate, V_s is the source voltage, C_{FOX} is the parasitic capacitance between the floating gate and the bulk, V_B is the bulk voltage, C_{OX} is the capacitance between channel and the floating gate, Q_{FG} is any charge that can be present on the floating gate, and K_{CG} is the coupling coefficient.
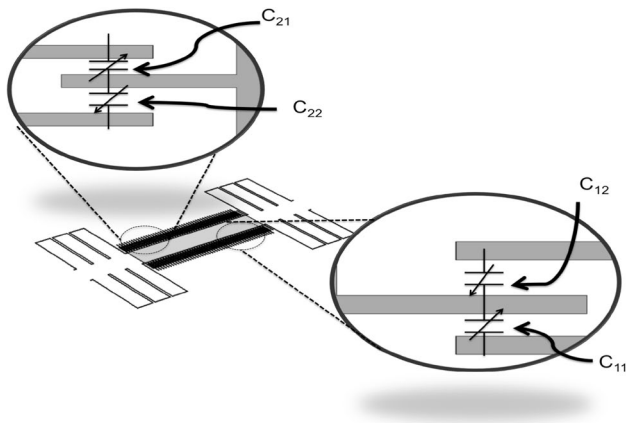
Fig. 2 Comb drive details

If we consider the parasitic capacitances present in the FGMOS, it is important to take into account that the total capacitance given by the inertial structure must be of the same order of magnitude of the total capacitance. This is, if $C_G \approx C_{TOT}$, the floating gate voltage will be the same as the transistor's gate voltage. Hence, C_G will not have any effect in the transistor; on the other hand, if $C_G \ll C_{TOT}$, the operation regime of the transistor cannot be controlled by changing C_G. Therefore, a good tradeoff is needed with design considerations in order to have a suitable operation of the transducer.

According to this situation, it is possible to suggest as a design consideration, that C_G should be an entire multiple of the sum $C_D + C_S + C_{FOX} + C_{OX}$. With this consideration the transduction of inertial force into an electric current is possible by means of an FGMOS, since the rest of the capacitors have a fixed value. Then, from (1) it can be deduced that any change on the coupling coefficient will cause V_{FG} to be variable, making it possible to correlate the inertial force with the drain current of the FGMOS transistor. In order to obtain an inertial structure which can operate based on this capacitive transduction, the spring design is important since the interaction between the plates affect the capacitors for coupling the control gate voltage over the floating gate. The main challenge of this design is to get the right mechanical characteristics in order to have a useful electrical performance.

In general, a MEMS accelerometer device can be divided into 3 parts: (a) the proof or seismic mass (b) the u–shaped springs/tethers, and (c) the inter–digitated comb structures (Bao 2005). For all the structures presented in this work, the seismic mass will have comb drives in order to achieve a variable value for C_G; the comb drives on each side of the mass will have a configuration as is shown in Fig. 2, which allows sensing acceleration in both directions along the moving axis, by means of a non–symmetrical distribution between fingers ($C_{12} < C_{11}$ and $C_{22} < C_{21}$) on the comb drives and a set of two FGMOS transducers.

3 Design considerations for the inertial sensor

In the structures based on the CMOS process mentioned previously, two polysilicon layers and three metal layers are available. The main advantage of using metal layers to fabricate the inertial sensors instead of polysilicon layers is that the thickness of the first two metal layers together is $\approx$1.75 μm whereas the polysilicon layers are 0.4 μm thick each, making it difficult to achieve a good performance structure if these layers are used. Other advantage of this kind of design is that it is not necessary to perform anisotropic bulk silicon etch since the parasitic capacitance between metal layers and bulk is smaller than the parasitic capacitance between the polysilicon layers and bulk.

MEMS based capacitive accelerometers are normally connected to CMOS circuits for capacitance sensing and providing electrical output for further signal processing (Mukherjee et al. 2012). In most cases, not only the electronic interface circuit requires dc bias, but also the capacitive structure. This dc bias causes the proof mass to move due to electrostatic actuation and usually this effect is an advantage to make self–test structures, but in this case due to the coupling between the capacitive structure and the FGMOS, it is considered an undesired effect, because the voltage across the sensing fingers may cause undesired movement of the structure, like pitch, yaw and roll, and also the fringe field effect is present due to the small distance between fingers in the comb drive.

In order to verify the effect of the electrostatic force, some considerations are made: only one face of the finger is fixed, the combs are divided in two principal groups; a comb which will be fixed to the transistor and another comb that will be part of the seismic mass. The dielectric characteristics are very important, since the electric field is the main source of noise present in the system, in this case the dielectric is considered as air in order to allow the free movement in the finger or in the capacitive structure. This consideration raises the complexity of the simulation since the surrounding air cannot be considered as solid and the finite elements that model the dielectric must have a free deformation characteristic in order to conserve continuity in the model that the solver uses. For each iteration, the finite element mesh for the dielectric must be recalculated because the solid is a deformable element. In this case, at each analysis step the capacitive structure of the fingers changes the stress and the displacement until the solver converges to the solution for a given applied force and voltage. The structure used for simulation in COMSOL® is shown in Fig. 3.

For this study, the mobile comb is biased with a variable voltage, and the fixed comb is set to ground. The dielectric considered is air, since the normal operation of the accelerometer will have very similar characteristics.
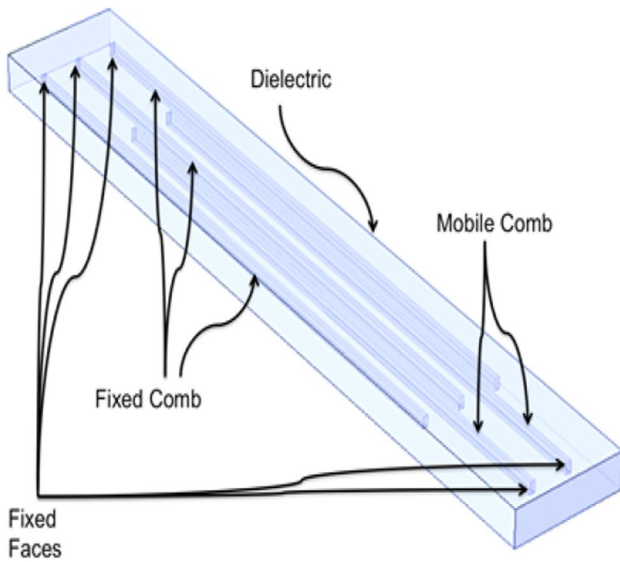
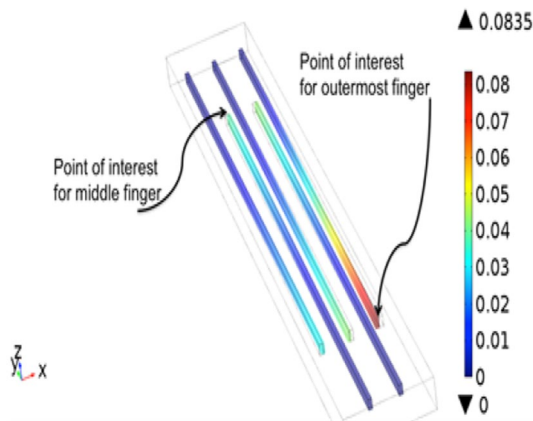Fig. 3 Comb drive configuration for COMSOL® Simulation

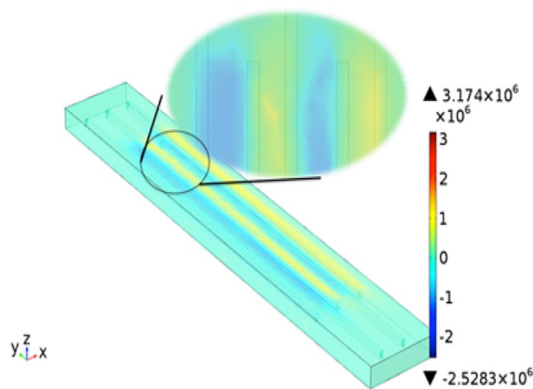Fig. 4 Displacement on x axis, with 5 V applied, overlap length 80 μm

Fig. 5 Electric field on x axis with 5 V applied, finger length 100 μm
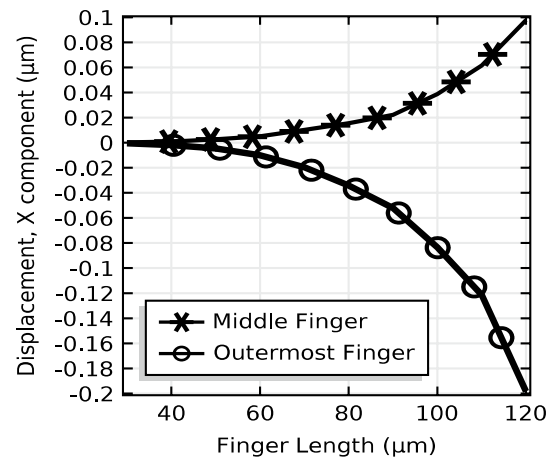

Fig. 6 Displacement on x axis on the point of interest, with 2.5 V applied

The results for the displacement and the electric field are shown in Figs. 4 and 5. It can be seeing, from Fig. 4 that the larger displacement corresponds to the outermost finger that has the smaller gap capacitor, this larger displacement is because it has no electric field in opposite direction on each side, as can be seeing in Fig. 5.

In order to verify how the middle fingers move when a voltage is applied between them, a parametric sweep was carried out, changing the applied voltage between the combs, from 0 to 30 V; the displacement of the middle fingers is the same for this voltage range since they have their respective counterpart fingers on each side to compensate the displacement, only the outermost fingers at each side of the array will not have their respective counterpart, so that the displacement is larger. The displacement on the far end part of the middle finger could be considered as constant, since the electrostatic force is too small to overcome the stiffness coefficient.

If the length of the finger increases, the expected displacement will increase as shown in Fig. 6. The displacement of the outermost finger is more significant than the rest of the fingers, in order to prevent these fingers from contacting with the opposite electrode.

Consequently, the outermost finger will constrain the maximum applied voltage, together with the maximum finger length, in order to avoid the electrodes to stick together. However, the displacement of the middle fingers will be the one that determines the value of C_G. From Fig. 6 it can be concluded that the stiffness coefficient has an important role in the behavior of the system and if a more precise performance is desired, the springs supporting the seismic mass must be modeled, since the effect of the electrostatic force and gravity over this mass will highly depend on the design.
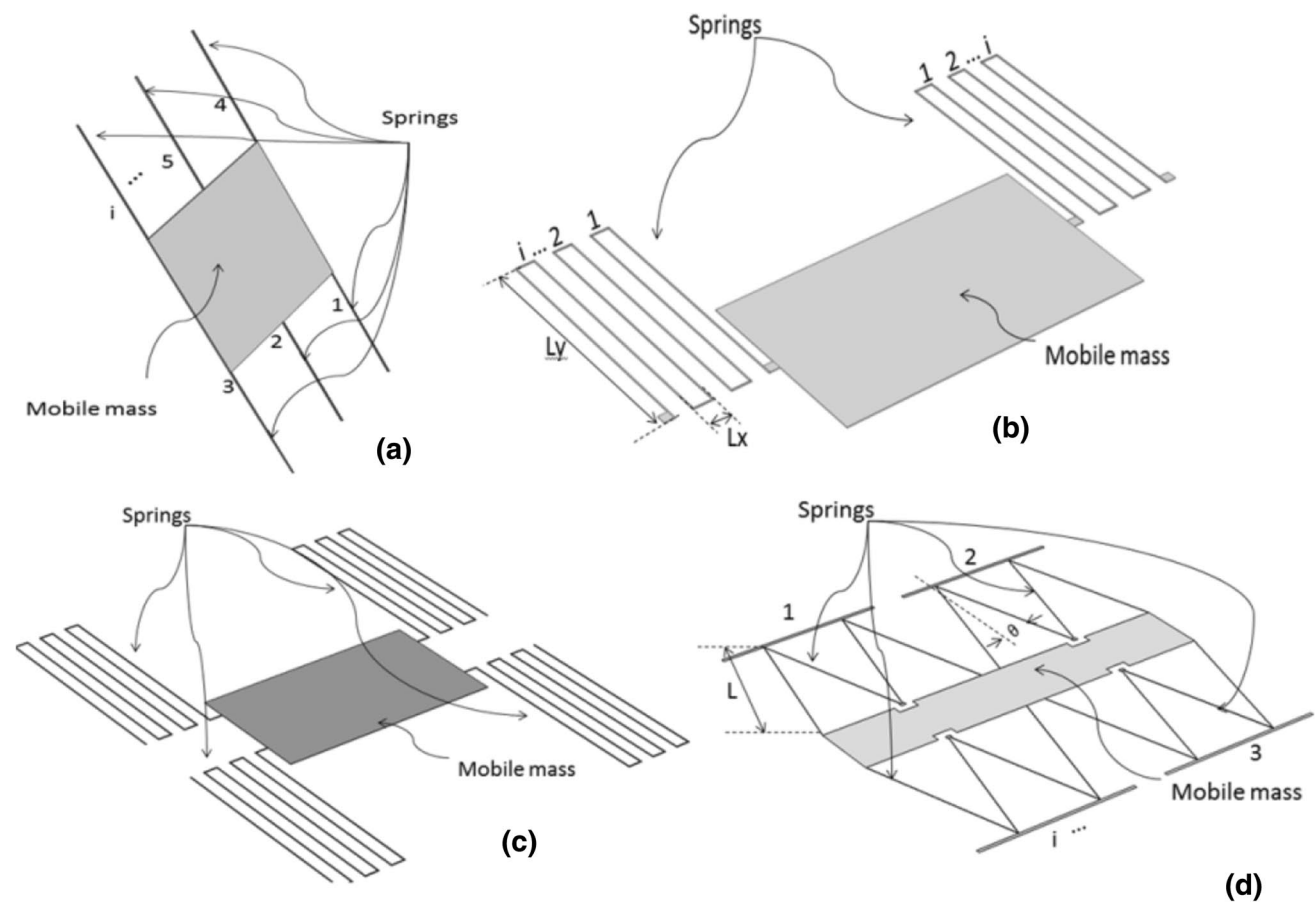
Fig. 7 Capacitive structures

For this kind of structures it is necessary at least two supports in order to minimize the pitch, roll and yaw. The design will be governed by some requirements, i.e. the area should be small, the effect of gravity on the seismic mass must be minimal, and the springs need to be flexible enough to allow a good displacement for the variable capacitor yet stiff enough to avoid undesired vibration. The structures observed in Fig. 7, were calculated to use the minimum occupied area, following the VLSI philosophy.

Due to the proposed geometry and configuration of the structures, the range of the variable capacitor depends on factors like the magnitude and direction of the applied inertial force, the stiffness coefficient of the springs and the polarization voltage due to the electrical configuration. The stiffness coefficient that must be considered for the springs in this analysis is long the principal motion axis, x in the case presented, representing a longitudinal movement of the seismic mass. However, depending on the flexural stiffness of the structure, the mechanical properties of the material and the applied voltage, there can be different possibilities of displacement of the moving plate that should be considered in the analysis.

It is worth noting that the variable capacitance of interest is formed by the lateral walls of the fingers coming from the fixed part and from the proof mass. However, as mentioned before, the capacitance will have different values if the moving plate moves across undesired axes, since the plates overlap will be different. So, these displacements should be minimized and the movement along the x axis must be enhanced while designing the structure. A detailed analysis will show the effect of the movement along different axes upon the target capacitance.

A very important mechanical constrain is the maximum displacement allowed by the springs; if a very large displacement is considered in order to maximize the rate of change of the capacitor, the motion along undesired axes will increase and this affects the expected capacitance. The displacement along the desired axis should be at most one-third of the distance between the electrodes at rest (with no external force applied to the structure) (Kaajakari 2009). In this case the principal axis of movement considered will be the x axis, so the displacement along it must be limited as follows:

$$x < \frac{1}{3}d \qquad (4)$$

where x is the displacement of the structure along the x axis and d is the gap between the capacitor electrodes. This limitation on displacement serves not only to avoid the undesired movement on the rest of the axes (yaw, pitch and roll), but also to avoid the oscillation along the *x axis* when the seismic mass has been displaced from the equilibrium position and returning to the rest position.

The next consideration is the pull in voltage, which can be calculated by:

$$V_p = \sqrt{\frac{8}{27}\frac{kd^3}{\epsilon_0\,A}} \qquad (5)$$

where V_p is the pull in voltage, k represents the spring constant over the axis of interest, A corresponds to the overlap area between the capacitors plates and ϵ_0 is the vacuum permittivity.

Furthermore, the electrostatic force on each axis could change the final value on the capacitive structure; the involved forces on each axis considering the applied voltage, can be calculated by:

$$\sum_x F = \frac{1}{2}\frac{\partial CG_{ii}(x,y,z)}{\partial x}V^2 + K_x x = 0 \qquad (6)$$

$$\sum_y F = \frac{1}{2}\frac{\partial CG_{ii}(x,y,z)}{\partial y}V^2 + K_y y = 0 \qquad (7)$$

$$\sum_z F = \frac{1}{2}\frac{\partial CG_{ii}(x,y,z)}{\partial z}V^2 + K_z z + mg = 0 \qquad (8)$$

where V is the applied voltage, $K_x x$ is the inertial force in the x axis, $K_y y$ is the inertial force in the y axis, $K_z z$ is the inertial force in the z axis, mg is the force due to gravity and CG_{ii} is the capacitor on each side of the comb drive. Therefore, the change on the final value of the capacitor will depend on the applied voltage, the stiffness coefficient of the springs on each axis, and the displacement due to gravity.

4 Results and discussion

Four different designs of the structure were analyzed and the results for this mechanical analysis are presented below. In Figs. 8, 9, 13 and 14 the displacement for each structure considering inertial force (6G) and gravity is shown. The
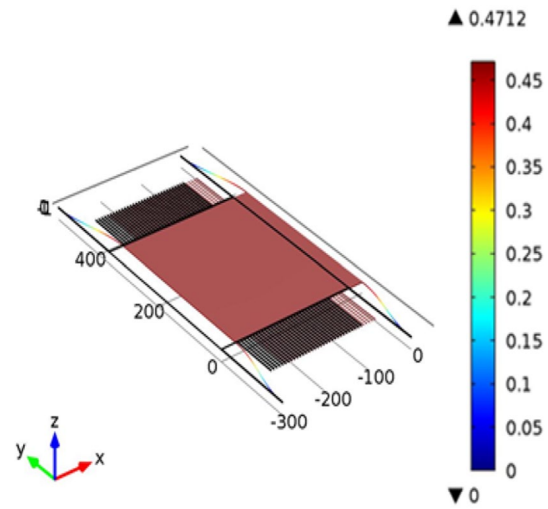

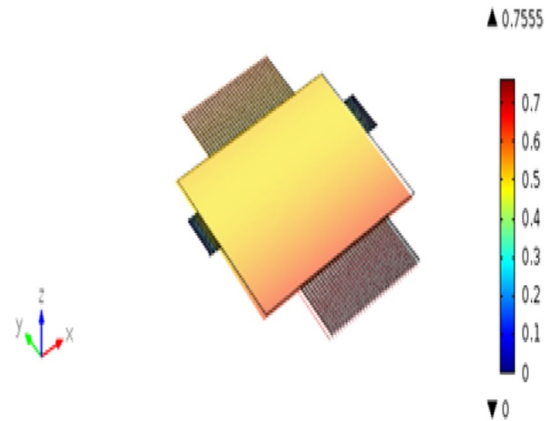**Fig. 8** COMSOL® simulation: capacitive structure (a) with maximum inertial force (6G) applied

Fig. 9 COMSOL® simulation: capacitive structure (b) with maximum inertial force (6G) applied

Table 1 Specifications set used for the capacitive structures

Parameters	Values	Units
V_p: pull in voltage	5.98	V
ω: beam width	0.9	μm
K_x: spring constant in x axis	0.06	N/m
d1: electrodes gap	2	μm
d2: electrodes gap	3	μm
x: maximum expected displacement in x axis	0.5	μm
h:thickness	1.75	μm
E:Young's Modulus	70×10^9	Pa
F: maximum inertial force	58.86	N
m: movable mass weight	5.17×10^{-11}	kg
A:overlap area in rest	1.75×80	μm²

Fig. 10 Capacitance vs. acceleration in structure (a) due to inertial force on three axes
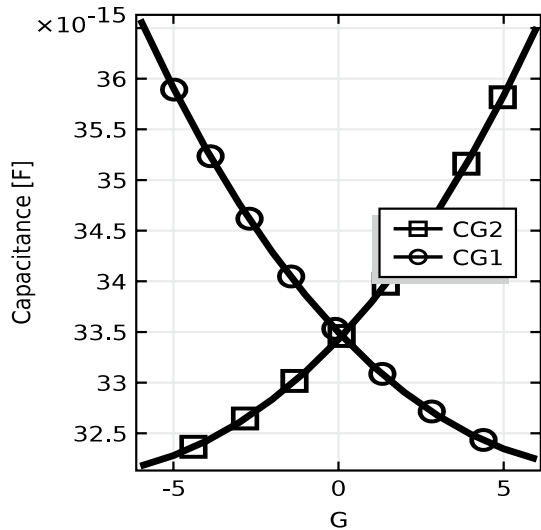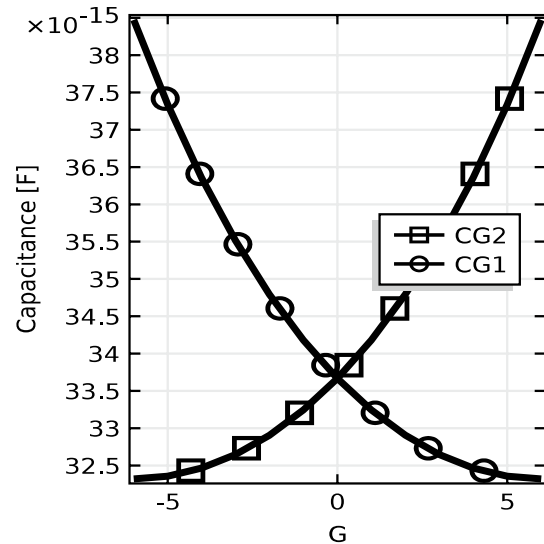

Fig. 11 Capacitance vs. acceleration in structure (b) due to inertial force on three axes

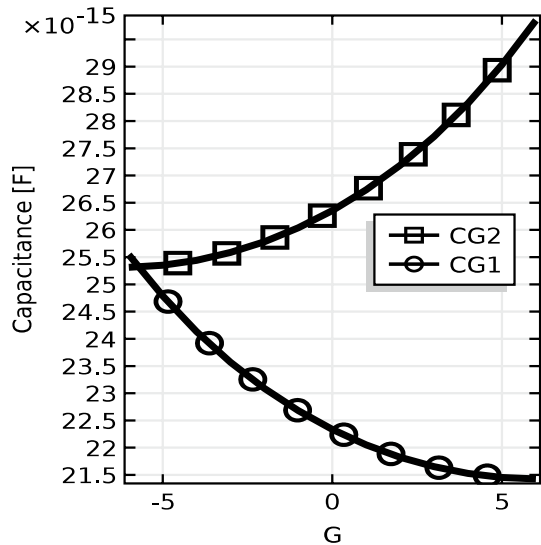**Fig. 12** Capacitance vs. acceleration in structure (c) due to inertial force on three axes

Fig. 13 COMSOL® simulation: capacitive structure (c) with maximum inertial force (6G) applied
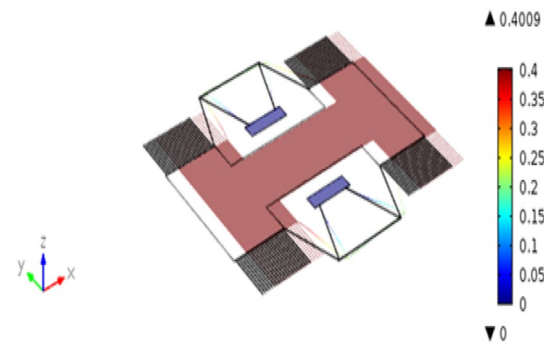
Fig. 14 COMSOL® simulation: capacitive structure (d) with maximum inertial force (6G) applied

specifications set used for the four structures (Fig. 7a–d) are shown in Table 1.

The capacitors C_{G1} and C_{G2}, are the capacitors which were formed on each side of the seismic mass and their respective fixed counterpart (see Fig. 2). While the capacitance C_{G1} increase, C_{G2} decreases and viceversa. This capacitance shown in Figs. 10, 11, 12 and 15 is due to the displacement of the seismic mass due to movement along the three axes (not only the desired approach along the x axis, but also the undesired yaw, pitch and roll movements).

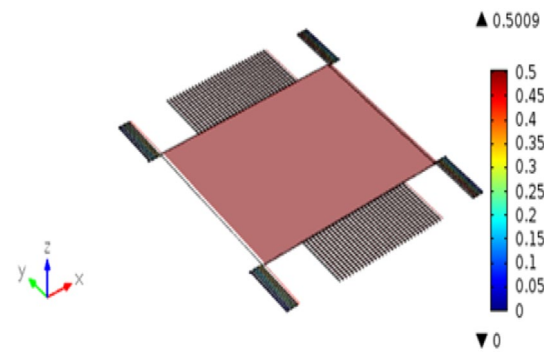As can be seen from Figs. 8, 9, 13 and 14 the total displacement is very different on each structure; for structure A, the expected displacement (0.5 μm) is different to that obtained from simulation (0.45 μm, see Fig. 8), but the capacitance variation is very symmetric.
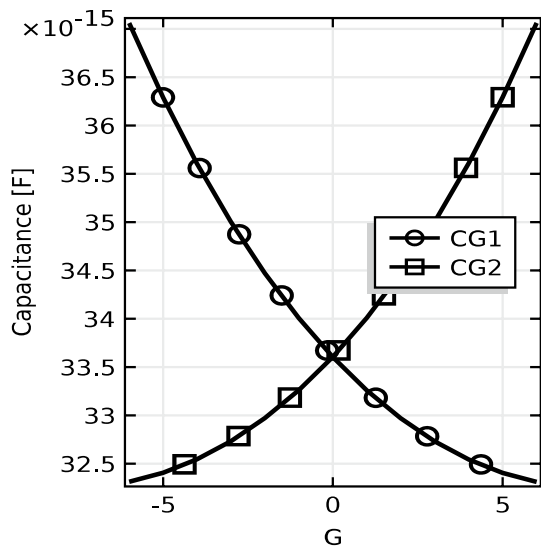
Fig. 15 Capacitance vs. acceleration in structure (d) due to inertial force on three axes

For structure B a small difference can be seen between the displacements along the *y axis*, with the pitch, roll and yaw movements present; this is reflected in the change of total capacitance. Regarding structure C the displacement is very similar from the expected value, and the capacitance is uniform and symmetric along the tree axes, also it has a larger range of capacitance compared with the other three structures. Next, structure D has a very similar behavior as structures A and C, but in contrast it has the disadvantage that its geometrical complexity presents several issues concerning the design rules of commercial CMOS technologies, so this option is discarded for fabrication.

From Figs. 10, 11, 12 and 15 it can be seen that when no force is applied, the total capacitance is different on each structure since the mechanical characteristics are also very different, despite the same stiffness coefficient is used throughout the design. The symmetry on the capacitance behavior is important in order to obtain a sensor response
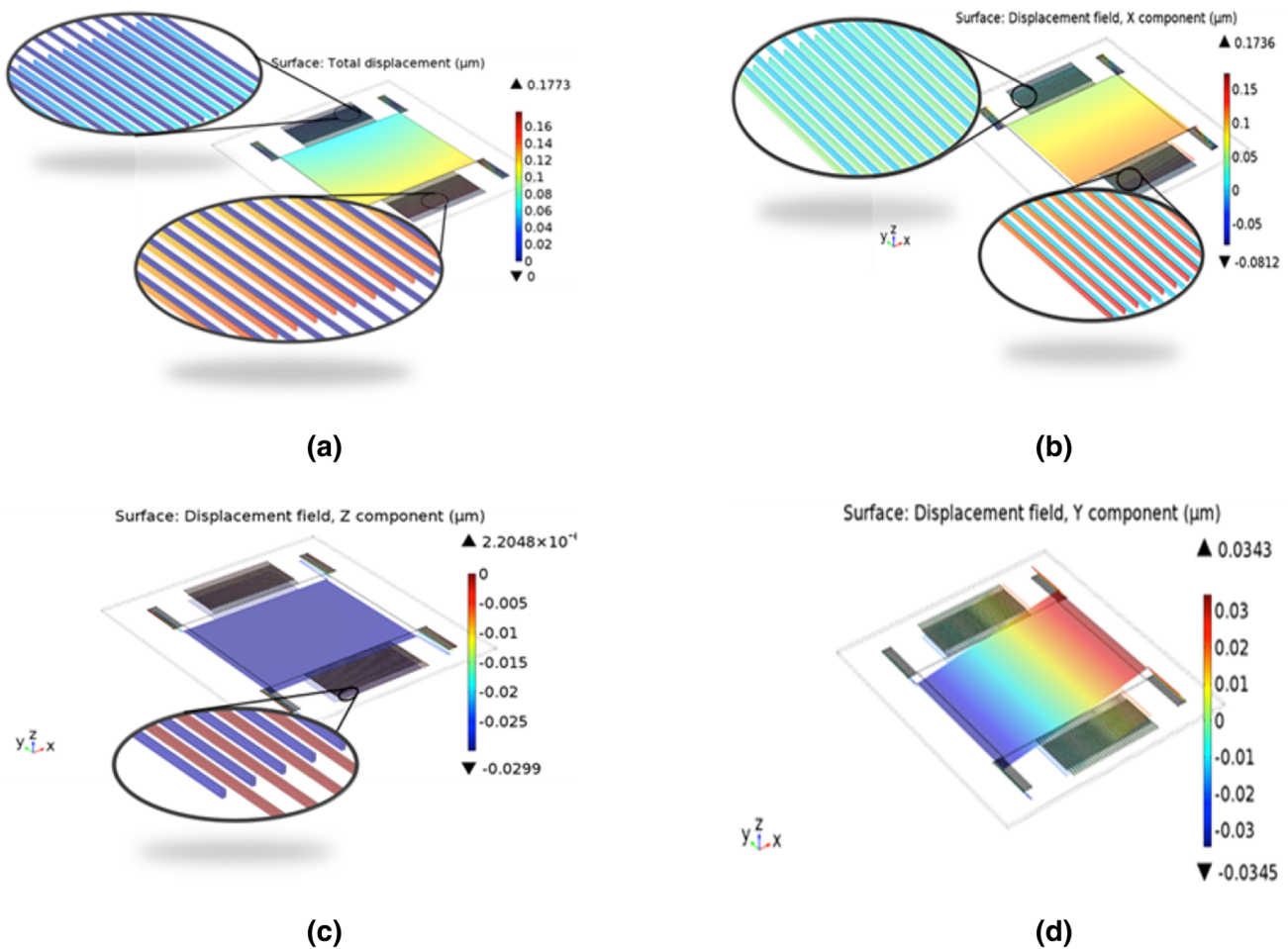

(a)

(b)

(c)

(d)

Fig. 16 (**a**) Total displacement (μm) due to electrostatic and body load. Displacement due to electrostatic actuation and body load in (**b**) x axis (roll), (**c**) z axis (yaw) and (**d**) y axis (pitch)
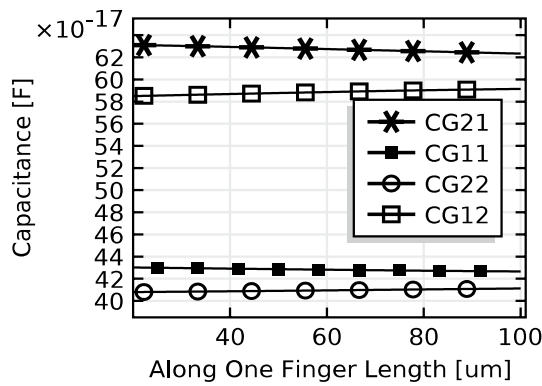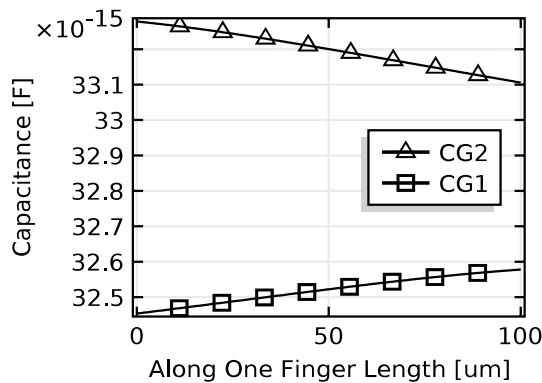
Fig. 17 Capacitance along one finger

Fig. 18 Capacitance ratio along fingers

as linear as possible. Considering structure C, from Fig. 12, it can be seen that this structure offers a larger change in capacitance; thereby this design allows higher resolution of the accelerometer.

A more detailed analysis was made using structure C, biasing the seismic mass with 5 V and the fixed fingers with 2.5 V; to verify the change on capacitance due to electrostatic actuation and the effect of gravity was included also as a body load, as these forces will change the capacitance of the structure despite no inertial force is being applied in this analysis. As it can be seen from the electro-mechanical analysis in Fig. 16 the pitch, yaw and roll movements are present on the structure.

From the electro-mechanical analysis, the undesired electrostatic actuation can be seen; furthermore, with gravity considered, the analysis also shows that the displacement along all the axes is not uniform. In Fig. 17, the change on capacitance along fingers C_{G21} and C_{G22}, which correspond to the capacitors formed on one side of the structure, can be seen, noting that at each side of the middle beam, two capacitors are present, one smaller than the other making possible to establish the direction of movement on the seismic mass; on the other hand, C_{G11} and C_{G12} correspond to the capacitors

formed on the opposite side of the seismic mass (see Fig. 2). From Fig. 17, it is seen that the total capacitance will be different on each side of the structure, since yaw, pitch and roll are present when the electrostatic actuation is present.

From Fig. 18 it can be seen that despite the difference between C_{G11} and C_{G12}, and C_{G21} and C_{G22}, when the total capacitance is obtained (C_{G2} and C_{G1}) the symmetry is evident. And the effect of the finger length due to electrostatic force is of less importance, but it is still considered since the same ratio on total capacitance was expected.

5 Conclusions

In this work, four different structures were analyzed. Their behavior was observed after performing a simulation including first only the effect of the applied inertial force, and subsequently performing an electro-mechanical simulation adding the effect of the applied voltage used to bias the system and gravity, from which undesirable movements occur resulting in a deviation of the expected average value of capacitance.

The effect of the electrostatic force is strongly correlated with the stiffness coefficient, since it was demonstrated that using the same characteristics for the springs, for instance, cross section area, equivalent stiffness and supported mass, it results that the effect of the involved forces has a different impact over the different proposed geometries. From the results shown, it can be seen that the structure C results to have the better behavior among the others, since it achieved both a larger change in capacitance and a smaller misalignment between the structure fingers. Even though the capacitance range achieved is small, it fits good enough to appreciate a change over the floating gate voltage of the FGMOS. From this point of view, it is recommended not to go beyond the order of magnitude of the parasitic capacitance, since this may conduct to a reduction of the sensibility of the floating gate voltage, making the FGMOS useless as a transducer. Despite the capacitance ratio is not the same on each side of the structure, a change of the aspect ratio of the FGMOS can minimize this effect, and the range on the total capacitance may be larger to achieve a good performance of the FGMOS as a transducer.

This study also emphasizes the importance of simulation as an important step during the design of MEMS devices. If the design is restricted by technological constraints, this step allows testing several configurations to reach the most suitable one for the desired performance, such that the design includes the majority of the factors that affect the device being designed.

References

Andò B et al (2011) A BE-SOI MEMS for inertial measurement in geophysical applications. IEEE Trans Instrum Meas 60(5):1901–1908

Bao M (2005) Analysis and design principles of MEMS devices. Elsevier, Beijing

Hsu HJ, Huang JT, Lee KY, Tsai TC (2012) Development of UV-Liga contact probe. 7th International microsystems, packaging, assembly and circuits technology conference. Taipei: IEEE, pp 183–188

Kaajakari V (2009) Practical MEMS. Small Gear, Las Vegas

Khan F, Zhu Y, Lu J, Dao D (2013) Design of metal MUMPS based LLC resonant converter for on-chip power supplies. IEEE 8th conference on industrial electronics and applications, IEEE, pp 700–704

Lazarus N, Bedair S, Lo C, Fedder G (2010) CMOS–MEMS capacitive humidity sensor. J Microelectromech Syst 19(1):183–191

Mukherjee B, Swamy K, Kar S, Sen S (2011) Effect of voltage induced electrostatic forces on MEMS capacitive accelerometer. IEEE Students Technology Symposium IEEE, pp 253–258

Mukherjee B, Swamy K, Sen S (2012) A new approach for sensitivity improvement of MEMS capacitive accelerometer using electrostatic actuation. 6th International conference on sensing technology, pp 738–742

Sethuramalingam T, Vilmalajuliet A (2010) Design of MEMS based capacitive accelerometer. International conference on mechanical and electrical technology Singapore: IEEE, pp 565–568